ISSN 1674-1056
http://cpb.iphy.ac.cn
http://iopscience.iop.org/cpb
中国物理 B
Chinese Physics
中国物理 Chinese Physics B

Analysis of iris-loaded resonance cavity in miniaturized maser

Zu-Gen Guo(郭祖根), Yong Zhang(张勇), Tao Tang(唐涛), Zhan-Liang Wang(王战亮), Yu-Bin Gong(宫玉彬), Fei Xiao(肖飞), Hua-Rong Gong(巩华荣)
Citation: Chin. Phys. B . 2020, 29(5): 050601 . **doi:** 10.1088/1674-1056/ab7d98
Journal homepage: http://cpb.iphy.ac.cn; http://iopscience.iop.org/cpb

What follows is a list of articles you may be interested in

Development of the integrated integrating sphere cold atom clock

Ming-Yuan Yu(于明圆), Yan-Ling Meng(孟艳玲), Mei-Feng Ye(叶美凤), Xin Wang(王鑫), Xin-Chuan Ouyang(欧阳鑫川), Jin-Yin Wan(万金银), Ling Xiao(肖玲), Hua-Dong Cheng(成华东), Liang Liu(刘亮)
Chin. Phys. B . 2019, 28(7): 070602 . **doi:** 10.1088/1674-1056/28/7/070602

Ramsey-coherent population trapping Cs atomic clock based on lin||lin optical pumping with dispersion detection

Peng-Fei Cheng(程鹏飞), Jian-Wei Zhang(张建伟), Li-Jun Wang(王力军)
Chin. Phys. B . 2019, 28(7): 070601 . **doi:** 10.1088/1674-1056/28/7/070601

Photonic generation of RF and microwave signal with relative frequency instability of 10^{-15}

Lu-Lu Yan(闫露露), Wen-Yu Zhao(赵文宇), Yan-Yan Zhang(张颜艳), Zhao-Yang Tai(邰朝阳), Pan Zhang(张攀), Bing-Jie Rao(饶冰洁), Kai Ning(宁凯), Xiao-Fei Zhang(张晓斐), Wen-Ge Guo(郭文阁), Shou-Gang Zhang(张首刚), Hai-Feng Jiang(姜海峰)
Chin. Phys. B . 2018, 27(3): 030601 . **doi:** 10.1088/1674-1056/27/3/030601

Evaluation of the frequency instability limited by Dick effect in the microwave $^{199}Hg^{+}$ trapped-ion clock

Yi-He Chen(陈义和), Lei She(佘磊), Man Wang(汪漫), Zhi-Hui Yang(杨智慧), Hao Liu(柳浩), Jiao-Mei Li(李交美)
Chin. Phys. B . 2016, 25(12): 120601 . **doi:** 10.1088/1674-1056/25/12/120601

Microwave interrogation cavity for the rubidium space cold atom clock

Wei Ren(任伟), Yuan-Ci Gao(高源慈), Tang Li(李唐), De-Sheng Lü(吕德胜), Liang Liu(刘亮)
Chin. Phys. B . 2016, 25(6): 060601 . **doi:** 10.1088/1674-1056/25/6/060601

Analysis of iris-loaded resonance cavity in miniaturized maser*

Zu-Gen Guo(郭祖根), Yong Zhang(张勇), Tao Tang(唐涛), Zhan-Liang Wang(王战亮), Yu-Bin Gong(宫玉彬), Fei Xiao(肖飞), and Hua-Rong Gong(巩华荣)†

National Key Laboratory of Science and Technology on Vacuum Electronics, School of Electronic Science and Engineering, University of Electronic Science and Technology of China, Chengdu 610054, *China*

(Received 10 December 2019; revised manuscript received 1 March 2020; accepted manuscript online 9 March 2020)

The size reduction of atomic clocks is a long-standing research issue. Many atomic clocks such as passive hydrogen masers (PHMs) and compact rubidium masers (CRMs) use iris-loaded resonance cavities (IRCs) as their microwave cavities because they can dramatically reduce the radical sizes of the atomic clocks. In this paper, the electromagnetic characteristic of the IRC is investigated by a theoretical model based on electromagnetic field theory. The formulas to calculate the resonance frequency, quality factor, and magnetic energy filling factor are presented. The relationship between the IRC structure and its electromagnetic characteristic is clarified. The theoretical calculation results accord well with the electromagnetic software simulations and experimental results. The results in this paper should be helpful in understanding the physical mechanism of the IRC and designing the atomic clocks.

Keywords: maser, iris-loaded resonance cavity, resonance frequency, quality factor, magnetic energy filling factor

PACS: 06.30.Ft, 07.57.Pt, 84.40.Ua **DOI:** 10.1088/1674-1056/ab7d98

1. Introduction

Recently, there was an increasing interest in radically-miniaturized masers such as compact rubidium masers (CRM) and passive hydrogen masers (PHM), which are used as atomic clocks in communication and localization applications.[1–9] Iris-loaded resonance cavity (IRC) is widely used in these masers. Compared with cylindrical cavity and sapphire-loaded cylindrical cavity, the IRC can greatly reduce the radial size of atomic clock.[10–14] In addition, its excellent mechanical property makes it suitable for aerospace and mobile applications. Besides, the IRC has a broad field of applications in electron spin resonance (ESR), electron paramagnetic resonance (EPR), and nuclear magnetic resonance (NMR), where it is named split-ring or slotted-tube resonator.[6]

However, the structure of the IRC is very complex and thus it is difficult to analyze. At present, some electromagnetic simulation softwares are used to obtain the key parameters of IRC, such as resonance frequency, quality factor, and magnetic energy filling factor. Unfortunately, such an approach is time- and memory-consuming, and also difficult to understandits physical mechanism.[14] Its electromagnetic parameters are calculated by using a lumped-element circuit model and some simple formulas are obtained, but their accuracy is larger than 10% and does not satisfy actual requirement.

In this paper, a theoretical model based on electromagnetic field theory is set up to analyze the IRC. The formulas to calculate key electromagnetic parameters of the IRC are presented, such as resonance frequency, quality factor, and magnetic energy filling factor. Because electromagnetic wave concept is introduced into the analysis model, the physical mechanism is clearly expounded and the formulas to calculate key parameters are accurate enough for actual cavity design. Finally, the model and formulas are verified by both electromagnetic (EM) simulations and experimental results. Compared with sole EM simulation approach, the method proposed in this paper is fast as well as accurate.

2. Transmission-line model of IRC

The structures of the IRC for the CRM and the PHM are shown in Figs. 1(a) and 1(b), respectively. The former is a cylindrical cavity with some irises connected to the wall by straight fins. There are two lids at the ends of the cylindrical cavity, which are not shown in this figure for simplicity. The IRC for the PHM shown in Fig. 1(b) is almost similar to that in Fig. 1(a) except the circular fins. Both of the cavities consist of four outer cavities, one inner cavity and two end gaps. The outer cavity and inner cavity are coupled through the end gaps and the slots between the irises. The irises are capacitively-loaded electrodes used for reducing the resonance frequency. So the volume of the cylindrical cavity could be reduced meanwhile the resonance frequency is kept constant (for the resonance frequency of rubidium maser 6.834 GHz and the resonance frequency of hydrogen maser 1.420 GHz). The metal fins are used to connect irises to the cavity wall for mechani-

*Project supported by the National Natural Science Foundation of China (Grant No. 61371052).

†Corresponding author. E-mail: hrgong@uestc.edu.cn

© 2020 Chinese Physical Society and IOP Publishing Ltd

cal consideration. A thin-wall quartz cell is located in the inner cavity to store the active material (rubidium or hydrogen).

The IRC is a half-wavelength, open-circuited waveguide resonance cavity with a special cross-section shape.[16–19] The cavity operates at $TE_{01\delta}$ mode. If the cutoff wave number of the TE_{01} mode in the cross-section is determined, the properties of the IRC can be determined easily. The cutoff wave number k_c of this waveguide with a special cross-section shape can be obtained by the transverse resonance technique.[20] It is based on the fact that the field forms a standing wave in the transverse plane of the waveguide under the cutoff condition. In this case, the waveguide can be regarded as a resonant radial transmission line with an infinite axial length. The irises are capacitive-loaded discontinuities in the radial direction.

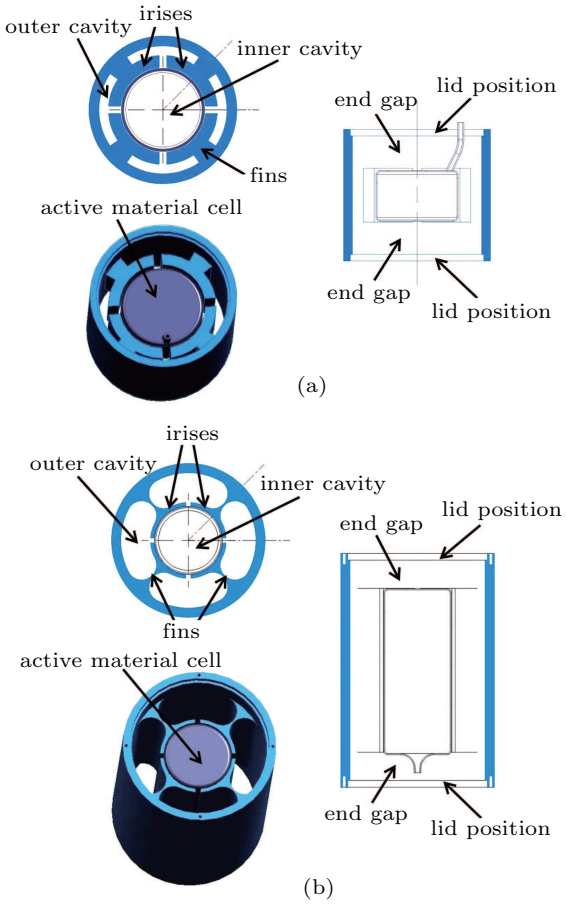


Fig. 1. Schematics of (a) IRC for CRM, and (b) IRC for PHM.

Due to the fact that the cavity structure is symmetric, we only consider a sector of the cross-section of the IRCs in the following analysis, and the results are shown in Fig. 1. For example, one sector of the IRC for the CRM is shown in Fig. 2(a). The angle of the iris is expressed as $\phi_1 = ((r_1+r_2)/2)/d$ approximately, where d is the slot length between the irises. In Fig. 2(b), one sector of the IRC for the PHM is shown. For simplicity, its semi-circular region is replaced by the region depicted by the dashed line in Fig. 2(b). Both the semi-circular region and the one depicted by the dashed line in Fig. 2(b) have the same area and thus their electromagnetic energy storage is almost equal in both cases. Therefore, the analysis model of the IRC for the PHM in Fig. 1(b) is the same as that in Fig. 2(a). In the following, we-analyze only the IRC for the CRM and the IRC for the PHM.

The structure in Fig. 2(a) can be treated as an iris loaded wedge-shaped radial resonant transmission line. The wave in this transmission line is in the TE-like mode. There are three important electromagnetic parameters in the design of the IRC, *i.e.*, resonance frequency, quality factor, and magnetic energy filling factor. In order to sustain the microwave field applied to the maser, the resonance frequency of the IRC should be consistent with the operating frequency of the maser. In addition, the properly chosen quality factor of the microwave cavity should guarantee a low power loss and the starting of oscillation. Finally, the homogeneity of the magnetic field inside the IRC in terms of intensity and orientation is crucial to the performance of the maser and it is represented by the magnetic energy filling factor. In the following, how to calculate these parameters will be discussed in detail.

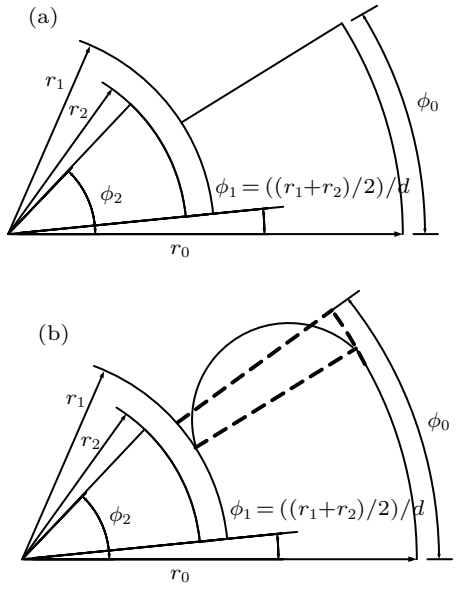


Fig. 2. (a) One sector of IRC for CRM and (b) one sector of IRC for PHM.

2.1. Resonance frequency

The wedged shape radial transmission line shown in Fig. 2(a) can be transformed into a parallel planar transmission line by implementing the conformal transformation as shown in Fig. 3. The admittance of the transmission lines and the equivalent circuit parameters of the iris are also shown in this figure. A reference plane is chosen at left side of iris. $^{-}\overline{Y}$ is the admittance seen into the left of the reference plane and $^{+}\overline{Y}$ is the admittance seen into the right. $\overline{B}_a$, $\overline{B}_b$, and $\overline{B}_c$ represent the equivalent circuit parameters of the iris.

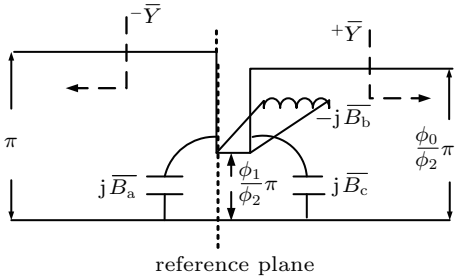


Fig. 3. Conformal transformation of transmission line with equivalent circuit parameters.

For the TE-like mode, the admittance of the radial transmission line can be written in the following form:[20]

$$^{-}\overline{Y} = -\mathrm{j}\frac{\mathrm{J}_0(k_\mathrm{c}r_2)}{\mathrm{J}_1(k_\mathrm{c}r_2)}, \tag{1}$$

$$^{+}\overline{Y} = \frac{Ct(k_\mathrm{c}r_1, k_\mathrm{c}r_0)\,\overline{Y}(r_0) + \mathrm{j}\zeta(k_\mathrm{c}r_1, k_\mathrm{c}r_0)}{\mathrm{j}\overline{Y}(r_0) - Ct(kcr_0, k_\mathrm{c}r_1)}, \tag{2}$$

where

$$Ct(k_\mathrm{c}r_1, k_\mathrm{c}r_0) = \frac{\mathrm{J}_1(k_\mathrm{c}r_0)\mathrm{N}_0(k_\mathrm{c}r_1) - \mathrm{N}_1(k_\mathrm{c}r_0)\mathrm{J}_0(k_\mathrm{c}r_1)}{\mathrm{J}_1(k_\mathrm{c}r_1)\mathrm{N}_1(k_\mathrm{c}r_0) - \mathrm{N}_1(k_\mathrm{c}r_1)\mathrm{J}_1(k_\mathrm{c}r_0)},$$

$$\zeta(k_\mathrm{c}r_1, k_\mathrm{c}r_0) = \frac{\mathrm{J}_0(k_\mathrm{c}r_1)\mathrm{N}_0(k_\mathrm{c}r_0) - \mathrm{N}_0(k_\mathrm{c}r_1)\mathrm{J}_0(k_\mathrm{c}r_0)}{\mathrm{J}_1(k_\mathrm{c}r_1)\mathrm{N}_1(k_\mathrm{c}r_0) - \mathrm{N}_1(k_\mathrm{c}r_1)\mathrm{J}_0(k_\mathrm{c}r_0)},$$

J_0 and J_1 are the first kind of Bessel function. N_0 and N_1 are the second kind of Bessel function. At the surface of the outside cavity, $\overline{Y}(r_0) = \infty$, so $^{+}\overline{Y} = -\mathrm{j}Ct(k_\mathrm{c}r_1, k_\mathrm{c}r_0)$.

The equivalent circuit parameters of the iris in Fig. 3 are determined by the following equations:

$$\overline{B}_\mathrm{a} = k_\mathrm{c}r_1\phi_2\frac{2}{\pi}\ln\left[\csc\left(\frac{\pi\phi_1}{2\phi_2}\right)\right] + \frac{\phi_2}{\phi_1}\tan\frac{(r_1-r_2)k_\mathrm{c}}{2}, \tag{3}$$

$$\overline{B}_\mathrm{b} = \frac{\phi_0+\phi_2}{2\phi_1}\csc((r_1-r_2)k_\mathrm{c}), \tag{4}$$

$$\overline{B}_\mathrm{c} = k_\mathrm{c}r_2\phi_0\frac{2}{\pi}\ln\left[\csc\left(\frac{\pi\phi_1}{2\phi_0}\right)\right] + \frac{\phi_0}{\phi_1}\tan\frac{(r_1-r_2)k_\mathrm{c}}{2}. \tag{5}$$

At any reference plane on the resonant transmission line, the sum of the input admittance seen looking into either side of the reference plane must be zero when the cavity is at a resonance state.[19] So the following condition must be satisfied, *i.e.*,

$$^{-}\overline{Y} + \mathrm{j}\overline{B}_\mathrm{a} + \frac{-\mathrm{j}\overline{B}_\mathrm{b}\cdot(\mathrm{j}\overline{B}_\mathrm{c} + {}^{+}\overline{Y})}{-\mathrm{j}\overline{B}_\mathrm{b} + (\mathrm{j}\overline{B}_\mathrm{c} + {}^{+}\overline{Y})} = 0. \tag{6}$$

Then, k_c can be obtained by solving this equation.

The end gap between the irises and the lid should be included in the resonance frequency calculation. Here, half of the iris-loaded resonance cavity in Fig. 1 is considered due to its symmetry along the axis direction. The analysis model is presented in Fig. 4, where L is the length of the end gap and h is the length of the iris.

The wave admittance on the left-hand side of the interface is as follows:

$$Y_\mathrm{I} = -\frac{\sqrt{k^2-k_\mathrm{c}^2}}{\mathrm{j}ck\mu\phi_1}\tan\left(\sqrt{k^2-k_\mathrm{c}^2}\cdot\frac{h}{2}\right), \tag{7}$$

where k is the free space wave number of the resonance frequency, c is the light speed in vacuum, and μ is the vacuum permeability.

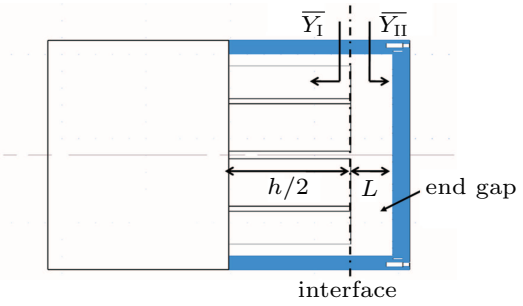


Fig. 4. Analysis model of cavity in axial direction.

The wave admittance on the right-hand side of the interface is

$$Y_\mathrm{II} = -\frac{\sqrt{k_{\mathrm{c}2}^2-k^2}}{\mathrm{j}ck\mu\phi_2}\cdot\frac{1+\exp\left(-2\sqrt{k_{\mathrm{c}2}^2-k^2}L\right)}{1-\exp\left(-2\sqrt{k_{\mathrm{c}2}^2-k^2}L\right)}\mathrm{e}^{1/n}, \tag{8}$$

where $k_{\mathrm{c}2}$ is the cutoff wave number of the TE_{01} mode in a cylindrical waveguide. $k_{\mathrm{c}_2} = p'_{01}/r_0$ where p'_{01} is the first root of the function $\mathrm{J}'_0(k_\mathrm{c}r_0) = 0$. Owing to the high-order modes excited by the end of the irises, a modification factor $\mathrm{e}^{1/n}$ related to the iris number n should be added into the expression. Because the resonance frequency of the IRC is lower than the cutoff frequency of the TE_{01} mode in cylindrical waveguide, the electromagnetic wave in the end gap is an evanescent wave and the propagation factor is an imaginary value.[21–23]

At resonance state, the wave admittance must be matched at the interface. Thus, we can obtain

$$\tan\left(\sqrt{k^2-k_\mathrm{c}^2}\cdot\frac{h}{2}\right) = \frac{\phi_1}{\phi_2}\cdot\frac{\sqrt{k_{\mathrm{c}2}^2-k^2}}{\sqrt{k^2-k_\mathrm{c}^2}}\cdot\frac{1+\exp\left(-2\sqrt{k_{\mathrm{c}2}^2-k^2}L\right)}{1-\exp\left(-2\sqrt{k_{\mathrm{c}2}^2-k^2}L\right)}\cdot\mathrm{e}^{1/n}. \tag{9}$$

The free space wave number k is obtained by solving this equation. The resonance frequency f is determined by $f = ck/(2\pi)$.

2.2. Quality factor

Due to finite conductivity of the cavity metal wall, the resonance frequency f, the free space wave number k and the cutoff wave number k_c will be complex, and then be denoted as $\overline{f}$, $\overline{k}$, and $\overline{k_\mathrm{c}}$ respectively. The quality factor of the cavity can be obtained through the following formula:[19]

$$Q = \left|\overline{f}\right| / \left|2\cdot\mathrm{Im}\left(\overline{f}\right)\right| = \left|\overline{k}\right| / \left|2\cdot\mathrm{Im}\left(\overline{k}\right)\right|. \tag{10}$$

Let $\overline{k_{\rm c}} = k_{\rm cr} + {\rm j}k_{\rm ci}$, where $k_{\rm cr}$ is the real part and $k_{\rm ci}$ the imaginary part. Due to $k_{\rm ci} \ll k_{\rm cr} \approx k_{\rm c}$, the complex free space wave number $\overline{k}$ can be calculated from Eq. (9) if the imaginary part of $\overline{k_{\rm c}}$, *i.e.*, $k_{\rm ci}$ is known.

On the inner surface of the outer cavity, $r = r_0$, owing to the lossy metal wall, the surface admittance is[24]

$$\overline{Y_{\rm m}}(r_0) = \frac{\eta k}{2Rk_{\rm c}}(1-{\rm j})\frac{1}{\rm j}\cot(1-{\rm j}) = \frac{\eta k}{2Rk_{\rm c}}(A+{\rm j}B), \quad (11)$$

where $A = 0.6505$, $B = -1.0856$, η is the wave impedance of vacuum, $R = \sqrt{\omega\mu/2\sigma}$ is the resistance of the cavity wall, and σ is the resistivity of the cavity material.

At the iris position, *i.e.*, $r = r_1$, the admittance in Eq. (11) is transformed into

$$\begin{aligned} {}^{+}\overline{Y} &= \frac{Ct(\overline{k_{\rm c}}r_1, \overline{k_{\rm c}}r_0)\cdot\overline{Y}_{\rm m}(r_0) + {\rm j}\zeta(\overline{k_{\rm c}}r_1, \overline{k_{\rm c}}r_0)}{{\rm j}\overline{Y}_{\rm m}(r_0) - Ct(\overline{k_{\rm c}}r_0, \overline{k_{\rm c}}r_1)} \\ &= -{\rm j}Ct(\overline{k_{\rm c}}r_1, \overline{k_{\rm c}}r_0) - \overline{Y}_{\rm m}(r_0)Ct(\overline{k_{\rm c}}r_1, \overline{k_{\rm c}}r_0)Ct(\overline{k_{\rm c}}r_0, \overline{k_{\rm c}}r_1) \\ &\quad + \frac{\zeta(\overline{k_{\rm c}}r_1, \overline{k_{\rm c}}r_0)}{\overline{Y}_{\rm m}(r_0)}. \end{aligned} \quad (12)$$

Similarly, the surface admittance on the left- and right-hand side of the iris are presented below:

$$\overline{Y}_{\rm ma} = \frac{\phi_2\eta k}{2(\phi_2-\phi_1)Rk_{\rm c}}(A+{\rm j}B), \quad (13)$$

$$\overline{Y}_{\rm mc} = \frac{\phi_0\eta k}{2(\phi_0-\phi_1)Rk_{\rm c}}(A+{\rm j}B). \quad (14)$$

Assuming that they are independent of the surface admittance and the thickness of the iris is neglected, the shunting capacitive elements of the iris are simplified into

$$\overline{B}_{\rm a'} = k_{\rm c}r_1\phi_2\frac{2}{\pi}\ln\left[\csc\left(\frac{\pi\phi_1}{2\phi_2}\right)\right], \quad (15)$$

$$\overline{B}_{\rm c'} = k_{\rm c}r_2\phi_0\frac{2}{\pi}\ln\left[\csc\left(\frac{\pi\phi_1}{2\phi_0}\right)\right]. \quad (16)$$

Thus, the total admittance on the iris is

$$\begin{aligned} \overline{Y}_{\rm a} &= \frac{1}{1/{\rm j}\overline{B}_{\rm a'} + 1/\overline{Y}_{\rm ma}} = {\rm j}\overline{B}_{\rm a'}\left(1 - \frac{{\rm j}\overline{B}_{\rm a'}}{\overline{Y}_{\rm ma}}\right) \\ &= {\rm j}\overline{B}_{\rm a'} + \frac{\left|\overline{B}_{\rm a'}\right|^2\cdot\dfrac{2(\phi_2-\phi_1)}{\phi_2}(A-{\rm j}B)}{\dfrac{1}{2}\dfrac{\eta k}{Rk_{\rm c}}|Z|^2}, \end{aligned} \quad (17)$$

$$\begin{aligned} \overline{Y}_{\rm c} &= \frac{1}{1/{\rm j}\overline{B}_{\rm c'} + 1/\overline{Y}_{\rm mc}} = {\rm j}\overline{B}_{\rm c'}\left(1 - \frac{{\rm j}\overline{B}_{\rm c'}}{\overline{Y}_{\rm mc}}\right) \\ &= {\rm j}\overline{B}_{\rm c'} + \frac{\left|\overline{B}_{\rm c'}\right|^2\cdot\dfrac{2(\phi_0-\phi_1)}{\phi_0}(A-{\rm j}B)}{\dfrac{1}{2}\dfrac{\eta k}{Rk_{\rm c}}|Z|^2}, \end{aligned} \quad (18)$$

where $|Z|^2 = |A|^2 + |B|^2$.

Regardless of the thickness of the iris, equation (6) is rewritten as

$${}^{-}\overline{Y} + \overline{Y}_{\rm a} + \overline{Y}_{\rm c} + {}^{+}\overline{Y} = 0. \quad (19)$$

Given $f(\overline{k_{\rm c}}) = {}^{-}\overline{Y} + \overline{Y}_{\rm a} + \overline{Y}_{\rm c} + {}^{+}\overline{Y}$, we obtain

$$f(\overline{k_{\rm c}}) \approx f(k_{\rm c}) + f(k_{\rm c})'({\rm j}k_{\rm ci}) = 0. \quad (20)$$

Then, we can obtain the imaginary part of the cutoff wave number from Eq. (20). Through some tedious manipulations, the imaginary part of $\overline{k_{\rm c}}$ can be written as

$$\begin{aligned} k_{\rm ci} &= \frac{A}{\dfrac{k\eta}{2k_{\rm c}R}|Z|^2}\cdot\left(\frac{Ct(k_{\rm c}r_1, k_{\rm c}r_0)Ct(k_{\rm c}r_0, k_{\rm c}r_1)}{D+\delta Ct}\right) \\ &\quad - \frac{A}{\dfrac{k\eta}{2k_{\rm c}R}|Z|^2}\cdot\left(\frac{\zeta(k_{\rm c}r_1, k_{\rm c}r_0)}{D+\delta Ct}\right) \\ &\quad - \frac{A}{\dfrac{k\eta}{2k_{\rm c}R}|Z|^2}\cdot\left(\frac{\dfrac{2(\phi_2-\phi_1)}{\phi_2}\left|\overline{B}_{\rm a'}\right|^2 + \dfrac{2(\phi_0-\phi_1)}{\phi_0}\left|\overline{B}_{\rm c'}\right|^2}{D+\delta Ct}\right), \end{aligned} \quad (21)$$

where

$$D = r_2\frac{\rm d}{{\rm d}x}\left(\frac{{\rm J}_0(x)}{{\rm J}_1(x)}\right)\Bigg|_{x=k_{\rm c}r_2},$$

$$\delta Ct = r_1\frac{\partial Ct(x,y)}{\partial x}\Bigg|_{\substack{x=k_{\rm c}r_1\\y=k_{\rm c}r_0}} + r_0\frac{\partial Ct(x,y)}{\partial y}\Bigg|_{\substack{x=k_{\rm c}r_1\\y=k_{\rm c}r_0}}.$$

When the loss on the side wall of the outer cavity is taken into account, a factor $k_{\rm ci2}$ should be added into the imaginary part of $\overline{k_{\rm c}}$,[25] and the resulting expression is as follows:

$$k_{\rm ci2} = \frac{Rr_1\delta Ct}{\eta r_1\phi_1(D+\delta Ct)}. \quad (22)$$

Since only the evanescent wave exists in the end gap, the loss in the end gaps is very small. It could be neglected in the quality factor calculation.

2.3. Magnetic energy filling factor

The magnetic energy filling factor measures the fraction of magnetic field energy useful for the clock signal with respect to the total microwave energy stored in the cavity. It is a measure of the efficiency of the cavity for coupling the overall microwave energy to the atoms stored in the cell, which is an important parameter for the maser, and this parameter is defined as[1]

$$\eta' = \frac{V_{\rm b}\langle H_z\rangle_{\rm b}^2}{V_{\rm c}\langle H^2\rangle_{\rm c}}, \quad (23)$$

where $V_{\rm b}$ and $V_{\rm c}$ are the volume of the active material cell and the volume of the total cavity, respectively. and H and H_z are the magnetic field and its axial component, respectively.

Because the field distribution is very complex in the cavity, it is difficult to obtain the value of the magnetic energy

filling factor precisely. However, since magnetic field is distributed mainly along the axial direction, integrating the H_z field in the cell of active material and all cavities will yield an approximate expression of the magnetic energy filling factor as follows:

$$\eta = \iiint_{V_{\text{cell}}} \left| \frac{\mathrm{J}_0(k_c r)}{\mathrm{J}_1(k_c r_1)} \right|^2 \mathrm{d}V \Big/ \left(\iiint_{V_{\text{in}}} \left| \frac{\mathrm{J}_0(k_c r)}{\mathrm{J}_1(k_c r_1)} \right|^2 \mathrm{d}V + \iiint_{V_{\text{out}}} \left| \frac{\mathrm{J}_1(k_c r_0)\mathrm{N}_0(k_c r) - \mathrm{N}_1(k_c r_0)\mathrm{J}_0(k_c r)}{\mathrm{J}_1(k_c r_1)\mathrm{N}_1(k_c r_0) - \mathrm{N}_1(k_c r_1)\mathrm{J}_1(k_c r_0)} \right|^2 \mathrm{d}V \right), \tag{24}$$

where V_{cell} is the volume of the active material cell, V_{in} and V_{out} are the volume of the inner and outer cavity, respectively.

3. Simulated and measured results

To verify the validity of the above analysis, an IRC example for the miniaturized PHM is presented, whose structural parameters are listed in Table 1. The electromagnetic characteristics of this IRC example are investigated by both the transmission-line model in the previous section and the EM simulation based on finite element method (FEM).[26] Here the eigenmode of HFSS is used to calculate the property of the IRC.

Table 1. Structural parameters of the IRC.

Parameter	Value
r_0/mm	60
r_1/mm	34
r_2/mm	31
d/mm	4.8
h/mm	145
L/mm	20
ϕ_0	0.2136π
ϕ_2	$0.25\ \pi$
Cavity material	aluminum
Surface roughness	0.4 μm

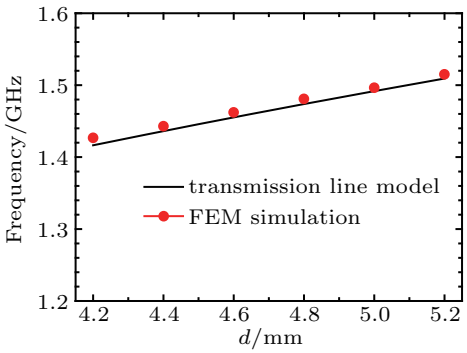


Fig. 5. Calculated and simulated variation of resonant frequency *versus* iris gap length d.

Figure 5 shows the calculated and simulated variation of resonant frequency *versus* the iris gap length. The calculated results agree well with those obtained by the EM simulation and the difference is less than 0.5%, which verifies the validity of the transmission-line model in this paper. As can be seen from Fig. 5, the resonance frequency can decrease as the length d of the iris gap decreases. Therefore, we can reduce the cavity size by reducing the iris gap while the resonance frequency remains unchanged.

Figure 6 shows the calculated and simulated variation of frequency *versus* end gap length L. Because the inner cavity and outer cavity are coupled through the magnetic line in the end gap, the decrease of the end gap length will increase the resonance frequency. In practice, it is convenient to adjust the resonance frequency by changing the end gap length.

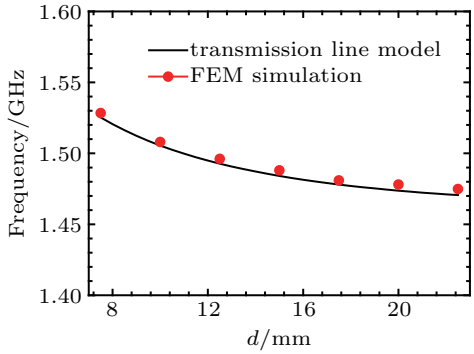


Fig. 6. Calculated and simulated variation of resonance frequencies *versus* end gap length L.

Figure 7 shows the calculated and simulated variation of quality factor *versus* iris gap length. The decrease of the iris gap will result in low quality factor of the cavity. So there is a tradeoff between the cavity size and the quality factor in the cavity design process. Because the loss at the end gap is omitted in the calculation, the calculated quality factor is larger than the EM one. However, the difference between them is less than 5% and it is good enough for actual design.

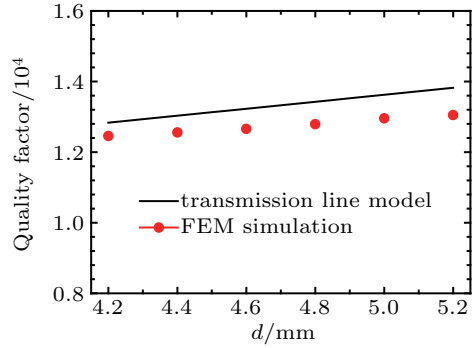


Fig. 7. Calculated and simulated variation of quality factor *versus* iris gap length d.

Figure 8 shows the calculated and simulated variation of magnetic energy filling factor *versus* iris radial location. By reducing the iris radial location, the magnetic energy filling factor slowly decreases. Figure 9 illustrates the magnetic field

in one quarter of the PHM cavity. It shows that the magnetic field is distributed mainly along the axial direction, as assumed in the analytic model. The calculated results agree well with the simulated ones.

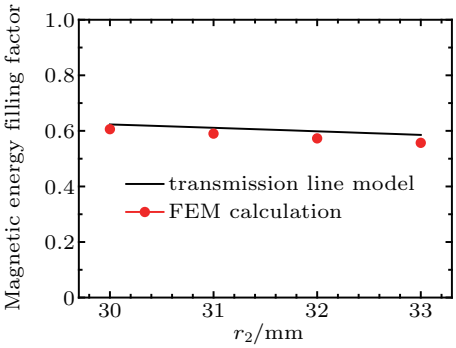


Fig. 8. Magnetic energy filling factor *versus* iris radial location.

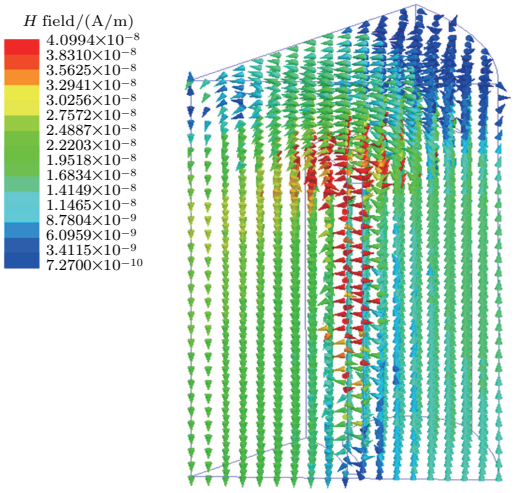


Fig. 9. Magnetic field distribution in PHM cavity.

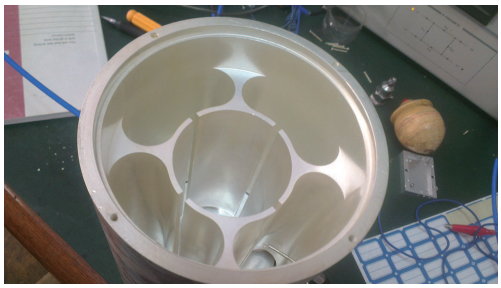


Fig. 10. Photograph of fabricated IRC for PHM.

Table 2. Calculated, simulated, and measured parameters of the PHM IRC.

Parameter	Calculated	EM simulated	Measured
Resonance frequency	1.474 GHz	1.485 GHz	1.480 GHz
Quality factor	1.70×10^4	1.65×10^4	1.00×10^4 (loaded Q factor, $S_{12} = 20$ dB)

Finally, a prototype IRC for the PHM is fabricated to verify the theoretical model in this paper as shown in Fig. 10. The structure parameters are the same as listed in Table 1 except the roughness of the cavity surface which is about 1 μm. A silver film is coated on the cavity surface by electroplating technique to increase the conductivity and the quality factor. In Table 2, the calculated, simulated, and measured results of the IRC for the PHM are compared with each other. They accord well with each other, which verifies the analysis in this paper.

4. Conclusions

Based on the electromagnetic field theory, a theoretical model for the IRC used in miniature maser is presented. The formulas to calculate its resonance frequency, quality factor, and magnetic energy filling factor are derived. As an example, an IRC for the PHM is presented and its electromagnetic parameters are calculated. The calculated results accord well with the simulated and measured results, which verifies the analysis. Compared with conventional methods, the proposed theoretical method is fast as well as accurate.

References

[1] Wang Q, Mosset P, Droz F, Rochat P and Busca G 2007 38*th Annual Precise Time and Time Interval (PTTI) Meeting* pp. 1–12
[2] Wang Y B, Yin M J, Ren J, Xu Q F, Lu B Q, Han J X, Guo Y, Chang H 2018 *Chin. Phys. B* **27** 023701
[3] Cheng P F, Zhang J W and Wang L J 2019 *Chin. Phys. B* **28** 070601
[4] Yu M Y, Meng Y L, Ye M F, Wang X, Ouyang X C, Wan J Y, Xiao L, Cheng H D and Liu L 2019 *Chin. Phys. B* **28** 070602
[5] Wang Q, Duan J, Qi X H, Zhang Y and Chen X Z 2015 *Chin. Phys. Lett.* **32** 54206
[6] Stefanucci C, Bandi T, Merli F, Pellaton M, Affolderbach C, Mileti G and Skrivervik A K 2012 *Rev. Sci. Instrum.* **83** 104706
[7] Zhuang Y X, Shi D T, Li D W, Wang Y G, Zhao X N, Zhao J Y and Wang Z 2016 *Chin. Phys. Lett.* **33** 40601
[8] Horsley A, Treutlein P, Mileti G, Affolderbach C, Du G and Bandi T 2015 *IEEE Trans. Instrum. Meas.* **64** 3629
[9] Xia B, Zhong D, An S and Mei G 2006 *IEEE Trans. Instrum. Meas.* **55** 1000
[10] Ivanov A, Bandi T, Du G X, Horsley A, Affolderbach C, Treutlein P, Mileti G and Skrivervik A K 2014 28*th Eur. Freq. Time Forum (EFTF)*, June, 2014, Neuchâtel, Switzerland, pp. 208–211
[11] Kang S, Gharavipour M, Affolderbach C, Gruet F and Mileti G 2015 *J. Appl. Phys.* **117** 104510
[12] Hartnett J, Tobar M, Stanwix P, Morikawa T, Cros D, and Piquet O 2005 *IEEE Trans. Ultrason. Ferroelect. Freq. Contr* **52** 1638
[13] Kang S, Affolderbach C, Gruet F, Gharavipour M, Calosso C E and Mileti G 2014 *Proc.* 28*th European Frequency and Time Forum (EFTF)*, June 22–26, 2014, Neuchâtel, Switzerland
[14] Peters H E 1978 32*nd Annual frequency Control Symposium*, 31 May–2 June, 1978, Atlantic, USA, p. 469
[15] Xue L, Dou W and Cao K 1984 *J. Chengdu Inst. Radio Eng.* Add Vol. **1–11**
[16] Annino G, Cassettari M and Martinelli M 2009 *IEEE Trans. Microwave Theory Tech.* **57** 775
[17] Sinclair K, Goussetis G, Desmulliez M, Sangster A, Tilford T, Bailey C and Parrott A 2008 *IEEE Trans. Microw. Theory Techn.* **56** 2635
[18] Chu Q, Ouyang X, Wang H and Chen F 2013 *IEEE Trans. Microw. Theory Techn.* **61** 1086
[19] Pozar D 2005 *Microwave Engineering*, 3rd edn. (Chichester: John Wiley and Sons)
[20] Marcuvitz N 1986 *Waveguide Handbook* (Stevenage, UK: Peregrinus)
[21] Montgomery G 1948 *Principles of microwave circuits* (Radiation Laboratory Series)
[22] Rong Y and Zaki K 2000 *IEEE Trans. Microw. Theory Techn.* **48** 258
[23] Sun W and Balanis C 1994 *IEEE Trans. Microw. Theory Techn.* **42** 2201
[24] Hopfer S 1955 *IRE Microwave Theory and Techniques* **43** 20
[25] March S 1985 *IEEE Trans. Microw. Theory Techn.* **33** 269
[26] HFSS *High Frequency Structure Simulator* (Los Angeles, CA: Ansoft Corporation)